From Wastes To Functions: Preparation of Layered Double Hydroxides From Industrial Waste And Its Removal Performance Towards Phosphates

Liping Xiao
Qingdao University of Technology
Yan Li
Liaoning Technical University
Qiaoping Kong (kongqiaoping@qut.edu.cn)
Qingdao University of Technology
Yunlong Lan
Qingdao University of Technology

Research Article

Keywords: Layered double hydroxides, Industrial waste residue, Phosphate, Adsorption, Wastewater

Posted Date: July 12th, 2021

DOI: https://doi.org/10.21203/rs.3.rs-633550/v1

From wastes to functions: Preparation of layered double hydroxides from industrial waste and its removal performance towards phosphates

Liping Xiao[a, *], Yan Li[b], Qiaoping Kong[a, *], Yunlong Lan[a]

[a] School of Environmental and Municipal Engineering, Qingdao University of Technology, Qingdao 266033, PR China

[b] School of Civil Engineering, Liaoning Technical University, Fuxin 123000, PR China

Abstract

To control eutrophication and recover phosphate from wastewater, a calcium carbide slag and red mud composite material (CR-LDH) was prepared using industrial waste as raw material for phosphorus adsorption. The morphology and structure of synthesized CR-LDH was characterized by FT-IR, SEM, EDS and XRD measurements. The experimental data can be well described by pseudo-second-order kinetics and Langmuir isotherm models, suggesting that the adsorption process of CR-LDH with respect to phosphate is a chemical and monolayer process. The theoretical maximum adsorption capacity obtained by Langmuir isotherm model is 16.06 $mg \cdot g^{-1}$ at 25 °C. The intra-particle diffusion model fitting results indicated that the adsorption of phosphate by CR-LDH was controlled by both liquid membrane

* Corresponding author at: School of Environmental and Municipal Engineering, Qingdao University of Technology, Qingdao 266033, PR China.

E-mail address: xxllpp11@126.com (L. P. Xiao); kongqiaoping@qut.edu.cn (Q. P. Kong)

diffusion and intra-particle diffusion. Phosphate was bound to CR-LDH via synergistic effect of physical adsorption, ion exchange, anion intercalation and chemical precipitation as evidenced from a combination of microscopic analysis and adsorption mechanism study. The actual phosphate-containing wastewater investigation showed that CR-LDH not only exhibited good removal effect on phosphate, but also could greatly reduce turbidity, COD and ammonia nitrogen, which was suitable for disposal of practical wastewater. These results indicate that CR-LDH can be considered as potential adsorbent for the treatment of phosphate-containing wastewater, which will be helpful to achieve the goal of "treating waste with waste and turning waste into treasure".

Keywords: Layered double hydroxides; Industrial waste residue; Phosphate; Adsorption; Wastewater

1. Introduction

As a non-renewable and irreplaceable resource, phosphorus is essential element for cell growth in plants, animals or bacteria, and thus necessary for maintaining the stability of the whole ecosystem (Jiang et al., 2019; Seftel et al., 2018). However, excess of phosphorous ($\geq$0.02 mg·L^{-1}) will cause eutrophication in widespread water body (Yang et al., 2019), along with a series of issues such as the reduction of water economic value and the the restriction of sustainable development of the society and economy. Hence, it's of vital importance for controlling redundant phosphate to a low level by cost-effective approaches (Zhang et al., 2019). Generally speaking,

phosphorus in wastewater usually exists in the main forms of organic phosphate, orthophosphate and polymeric (condensed) phosphate (Bacelo et al., 2020), but the total phosphorus content and the mass fraction of various forms of phosphorus vary depending on the source of the wastewater. Therefore, the most critical step in phosphorus removal of most wastewater is to consider how to remove orthophosphate.

Until now, various approaches have been adopted for the treatment of phosphorus-containing wastewater such as chemical precipitation, crystallization, biological processes and adsorption method (Bacelo et al., 2020). Among them, adsorption with the characteristic of simple operation, low cost and environment-friendly (Kong et al., 2021; Kong et al., 2019) is generally considered to be the most effective method for the treatment of phosphorus-containing wastewater. The key to the popularization and application of adsorption method lies in the research and development of cheap and efficient new adsorbents. Many kinds of adsorbents such as layered double hydroxides (LDHs) (Dox et al., 2019; Liu et al., 2019; Seftel et al., 2018; Zhang et al., 2019), zeolite (Li et al., 2021; Razmi and Ghasemi-Fasaei, 2018), corn bracts (Jiang et al., 2019), lignite (Samaraweera et al., 2021), aluminum-modified eggshells (Guo et al., 2017), sludge (Tie et al., 2013), MgO nanoparticles biochar composites (Zhu et al., 2021) and paper mill sludge-based calcium-containing porous biochar (Wang et al., 2021) have been reported for the removal of phosphorus from wastewater.

LDHs, also known as anionic clays, include hydrotalcite and hydrotalcite like

compounds, and the main body of LDHs is generally composed of hydroxides of two metals. LDHs have the properties of ion exchange between layers and permanent positive charge. After calcination, the product of LDHs has a huge specific surface area and can return to the original layered structure in a certain environment. LDHs is deemed as an excellent adsorbent for the removal of organic and inorganic pollutants from wastewater. In terms of phosphate removal, Zhang et al. successfully synthesized layered double hydroxides with nitrate via co-precipitation method and the experimental results showed that the multilayer structure of the synthesized LDHs exhibited good adsorption ability towards phosphate (Zhang et al., 2021). Jia et al. exfoliated and incorporated MgAlFe-LDHs in polyether sulfone membranes and the adsorption rate of the obtained membranes was faster than the un-exfoliated one. The adsorption capacity of obtained membranes with respect to phosphate was 5.61 $mg \cdot g^{-1}$ (Jia et al., 2018). Seftel et al. used modified ZnAl-LDHs to adsorb phosphate from aqueous solutions. The results showed that anionic exchange was the main adsorption mechanism for the phosphate adsorbed by non-calcined LDH, while the adsorption process of LDO materials towards phosphate was attributed to structural reconstruction and precipitation (Seftel et al., 2018). However, the LDHs used in most of the above publications were synthesized using chemical agents. If LDHs can be prepared from industrial waste, the production cost of adsorbent will be greatly reduced and the industrial waste can be reused for recycling. To our best knowledge, the literature focus on using industrial waste residue to prepare LDHs for the removal of phosphate from wastewater had rarely been reported.

85 The purpose of this study is to make full use of industrial waste residues to
86 develop new adsorbent for the removal phosphate in wastewater, which can reduce
87 the environmental pollution caused by industrial waste residues, and achieve the
88 purpose of effective treatment of phosphate-containing wastewater. Herein, we
89 prepared a novel CR-LDH adsorbent with hydrocalumite and magnesia structure by
90 calcium carbide slag and red mud via a simple method. Calcium carbide slag is a
91 calcium-containing solid industrial waste residue produced during the hydrride
92 process of chlor-alkali industry, and the main chemical components are CaO, Al_2O_3,
93 Fe_2O_3, SiO_2, MgO, etc. Red mud is a kind of solid waste residue in aluminum
94 industry formed from bauxite (Hu et al., 2017). The influencing factors of adsorbent's
95 dosage, pH and co-existing ions on the removal performance of phosphate were
96 discussed. The adsorption kinetics, isotherm and thermodynamics were systematically
97 studied. The adsorption mechanism was proposed by combining the experimental
98 investigation and characterization of CR-LDH before and after adsorption of
99 phosphate. In addition, the applicability of CR-LDH for the removal of phosphate in
100 practical phosphate-containing wastewater was also investigated.
101
102 **2. Materials and methods**
103 **2.1. Chemicals and materials**
104 The carbide slag was taken from an acetylene plant in Fuxin City,
105 Liaoning Province. The red mud was provided by an aluminum plant in
106 Liaocheng City, Shandong Province. The red mud used in this study is "Bayer

red mud" which accounts for more than 90% of the world's total red mud. The raw carbide slag and red mud were crushed and ground through 200 mesh sieve, and then dried to constant weight in 105 °C oven to remove the moisture and maintain the original properties of the materials. The picture of raw calcium carbide slag powder and red mud powder are presented in Fig. S1a and Fig. S1b of Supplementary Material, respectively. The chemical composition of raw calcium carbide slag powder and red mud powder are provided in Table S1 and Table S2. Potassium dihydrogen phosphate (KH_2PO_4) was purchased from Liaoning Quanrui Reagent Co., Ltd. 100 $mg \cdot L^{-1}$ phosphorus standard solution (GSB04-1741-2004a) was supplied by China's national center for analysis and testing of nonferrous metals and electronic materials. Ascorbic acid were purchased from Liaoning Quanrui Reagent Co., Ltd, China. The other chemicals were purchased from Shenyang Huadong Reagent Factory, China. All chemicals were of analytic grade (or higher), and were used without further purification.

2.2. Preparation of CR-LDH

The CR-LDH was prepared as the following steps: firstly, the raw material of calcium carbide slag and red mud were roasted at 600 °C for 3 h in muffle furnace, respectively. After cooling to room temperature, the obtained calcium carbide slag and red mud with mass ratio of 1:1 were fully mixed and then added into 300 mL deionized water. Under mechanical stirring of 700 $r \cdot min^{-1}$, the resulting slurry was stirred at 45 °C for 3 h. Subsequently, the above mixture was crystallized in 70 °C

129 water bath for 24 h and the residue was washed thoroughly with distilled water. After
130 drying at 105 °C to constant weight, the precipitate was ground to pass through
131 200-mesh sieve. Finally, carbide slag red mud composite powder was obtained,
132 denoted as CR-LDH. The picture of the prepared of CR-LDH was shown in Fig. S2.

133 **2.3. Physicochemical characteristic of CR-LDH**

134 The morphology and element distribution of CR-LDH was determined by a
135 S-4800 scanning electron microscopy (SEM) (Hitachi, Japan) and energy-dispersive
136 spectroscopy (EDS) mapping analysis. To determine the surface area of CR-LDH,
137 a ASAP2460 Brunauer-Emmett-Teller N_2 adsorption analysis (BET)
138 (Micromeritics, USA) was used. The functional groups and chemical bond types
139 of CR-LDH from 4000 to 400 cm^{-1} was measured by a NICOLET iS5 fourier
140 transform infrared spectroscopy (FT-IR) (Thermo Nicolet Corporation, USA). A
141 x'pert pro X-ray diffraction (XRD) (Spectris, Holland) with Cu K^{α} radiation (40
142 kV, 40 mA) at a scan speed of $4^{o}\cdot min^{-1}$ was used to detect the crystallographic
143 structure of CR-LDH.

144 **2.4. Batch adsorption experiments of CR-LDH**

145 A series of batch adsorption tests were conducted to evaluate the
146 adsorption performance of CR-LDH with respect to phosphate. The adsorption
147 experiments were carried out in 250 mL conical flasks with a certain amount of
148 CR-LDH and 100 mL of phosphate at 25 °C. After adsorption equilibrium, the
149 supernatants were collected and then filtered through 0.45 μm membrane filter and
150 diluted for further phosphate analysis by the UV spectrophotometer at a wavelength

of 700 nm using the molybdate colorimetric method (Zhang et al., 2019). The initial pH values of the phosphate solutions were adjusted by 0.1 mol·L^{-1} HNO_3 or NaOH. The adsorption kinetics of phosphate were carried out by immersing 0.5 g of CR-LDH into 100 mL phosphate solution with concentration of 30 mg·L^{-1} (25 ºC, 10 h). For the adsorption isotherms study, 0.5 g of CR-LDH was added into 100 mL of phosphate solution with initial concentration ranging from 5 to 210 mg·L^{-1} by maintaining reaction temperature at at 15, 25, 35 ºC, respectively. The adsorption amount and removal efficiency of CR-LDH towards phosphate were calculated by the following equations:

$$Q_t = \frac{(C_0 - C_t)V}{m} \quad (1)$$

$$\text{Removal efficiency} = \frac{(C_0 - C_t)}{C_0} \times 100\% \quad (2)$$

where Q_t is adsorption amount of phosphate onto CR-LDH at time of t, mg·g^{-1}; C_0 is the initial concentration of phosphate, mg·L^{-1}; C_t is the concentration of phosphate at time of t; m is the mass of CR-LDH, mg·L^{-1}; and V is the volume of solution, mL.

3. Results and discussion

3.1. Characterization of CR-LDH composites

The structural characteristics of calcium carbide slag, red mud and CR-LDH are investigated by XRD patterns and the results are shown in Fig. 1. In the spectrum of calcium carbide slag, the peaks at 2θ values of 18.107^0, 28.728^0, 34.169^0, 47.249^0, 50.896^0 and 54.464^0 suggested the presence of $Ca(OH)_2$. The component of $Ca(OH)_2$

would be conductive for the removal of phosphate by forming phosphide precipitation through the reaction between Ca^{2+} and phosphate at high pH environmental conditions. However, phosphate removal by calcium carbide slag would lead to higher pH value of effluent. The XRD pattern of red mud presented the absorption peaks of Fe_2O_3 ($2\theta=33.117^0$ and $2\theta=35.604^0$), CaO ($2\theta=24.749^0$ and $2\theta=29.756^0$) and SiO_2 ($2\theta=21.662^0$). The abundant metal elements in red mud, especially for Al and Fe, could interact with phosphate during the adsorption process. For XRD patterns of CR-LDH composite, the characteristic peaks corresponding to the (002) and (004) crystal planes of hydrocalumite were appeared, which was consistent with the PDF card of the International Diffraction Data Center (PDF#16-0333). The CR-LDH composite exhibited hydrocalumite structure. Hydrocalumite was an ordered layered inorganic compound of LDHs with excellent removal ability for phosphate. The diffraction peaks corresponding to the hydrocalumite (002) crystal plane had the characteristics of sharp peaks, good peak type, low and flat base line, high crystallinity and a relatively complete monoclinic symmetrical layered structure. In addition, the characteristic peaks corresponding to the (003) crystal face of boehmite were appeared in the XRD patterns of CR-LDH. The peaks of $CaCO_3$ ($2\theta=43.14^0$) and Fe_2O_3 ($2\theta=33.24^0$, $2\theta=35.73^0$ and $2\theta=54.21^0$) were also detected in the XRD patterns of CR-LDH. The reason for the existence of these metal oxides was that their raw materials are industrial waste slag, and the metal oxides were not fully reacted in the process of preparing the composites, and there were still some metal oxides in the CR-LDH composite. All these findings indicated that calcium carbide slag and red

mud ha been successfully compounded to form CR-LDH.

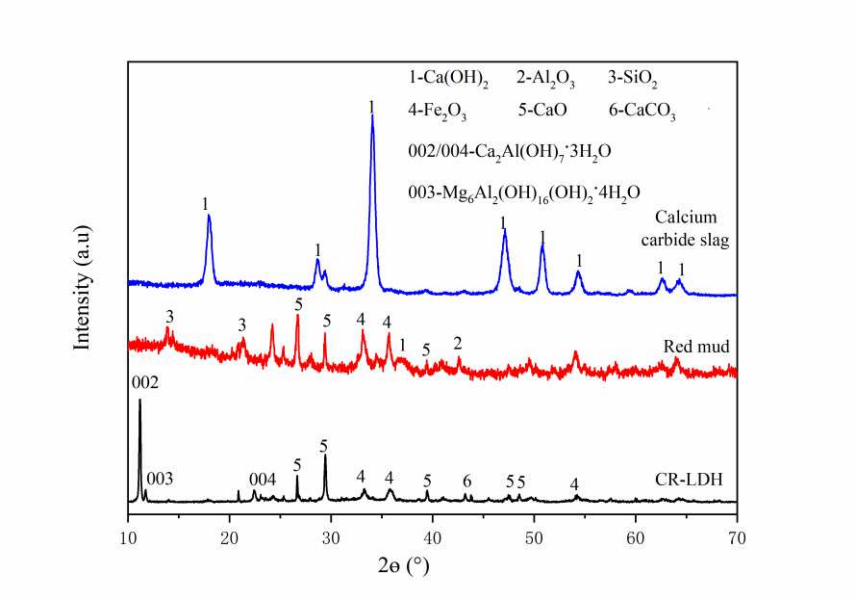

Fig. 1 XRD pattern of calcium carbide slag, red mud and CR-LDH.

SEM and EDS are used to investigate the surface morphology and element content distribution of CR-LDH, respectively. As shown in Fig. 2a and Fig. 2b, CR-LDH presented a typical plate-like morphology of LDHs (Cheng et al., 2019). The surface of CR-LDH was relatively rough and there are a large number of gaps, which was conducive to the adsorption process. The BET surface area of CR-LDH was 42.46 $m^2 \cdot g^{-1}$, providing a large number of surface active sites for the adsorption of phosphate in the aqueous solutions. According to the EDS results (Fig. 2c and Table 1), the content ratio of main elements of CR LDHs mainly contained O, Al and Ca, and the content of Ca was much higher than that of other metal elements, which were consistent with the XRD results that CR-LDH had the characteristic adsorption peaks of hydrocalumite and boehmite.

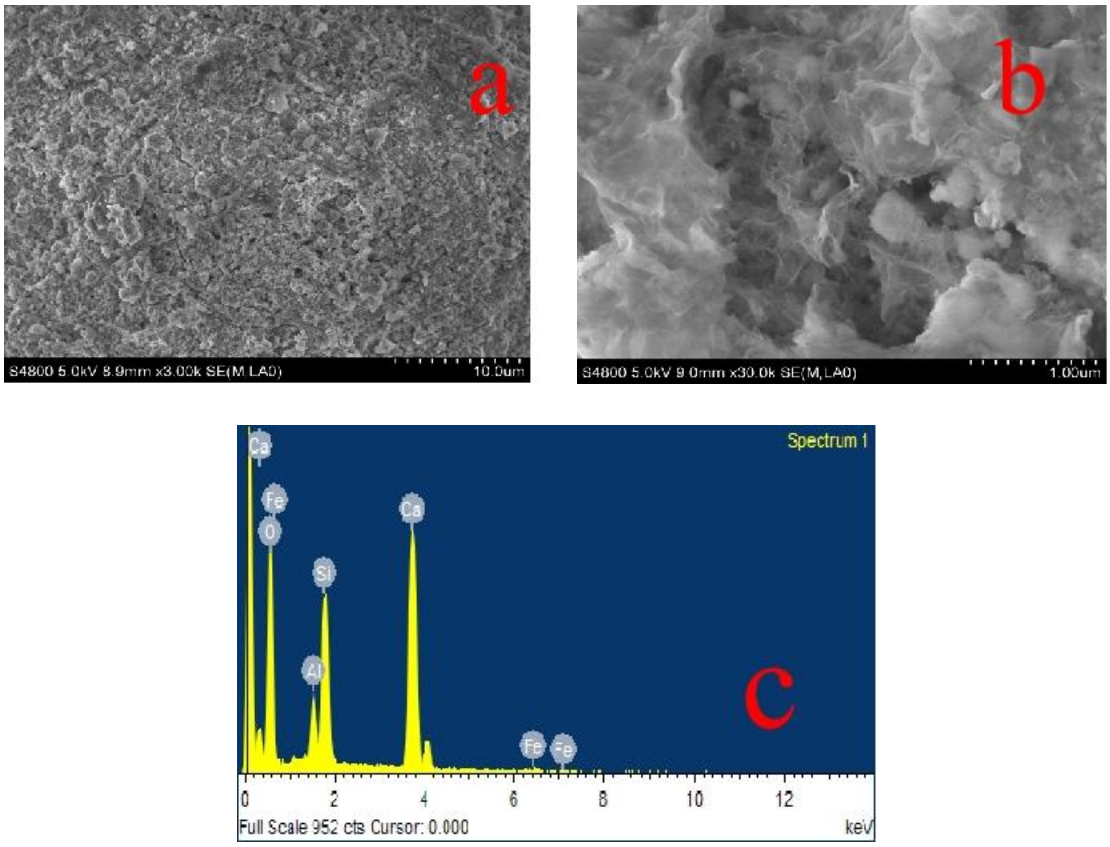

206 Fig. 2 SEM of CR-LDH (a, b) and EDS of CR-LDH (c).

207 Table 1 The elemental content changes of CR-LDH before and after adsorption of

208 phosphate.

Element	CR-LDH（Before adsorption）		CR-LDH-phosphate（After adsorption）	
	wt%	at%	wt%	at%
O	62.35	78.42	47.30	69.23
Al	3.26	2.43	7.49	6.50
Si	9.30	6.67	4.54	3.79
Ca	24.24	12.17	14.89	8.70
Fe	0.85	0.31	20.82	8.73

P	—	—	1.20	0.91

3.2. Optimization of the batch adsorption conditions

3.2.1. Effect of CR-LDH daosage on phosphate adsorption

To investigate the effect of dosage on the adsorption performance of CR-LDH with respect to phosphate, 0.5, 1, 2, 3, 4, 5 and 6 $g \cdot L^{-1}$ CR-LDH were added into 100 mL phosphate ion solution with a concentration 30 $mg \cdot L^{-1}$. Adsorption experiments conducted for 24 h at 25 ºC with pH of 7 and shaking speed of 180 $r \cdot min^{-1}$. The results are shown in Fig. 3a. It can be seen from Fig. 3a that the removal rate of phosphate was first gradually increased and then basically approached 100%, while the adsorption ability of per unit mass CR-LDH was gradually decreased. The increase of phosphate removal rate was due to the increase of adsorbent dosage, which increases the number of available adsorption sites on the material surface and the contact probability with adsorption sites in the solution, providing favorable conditions for phosphate adsorption removal. Under the condition that the initial concentration of phosphate is 30 $mg \cdot L^{-1}$, the amount of phosphate in solution was fixed and more phosphate were removed with the increasing dosage of CR-LDH, while the per amount phosphate adsorbed by CR-LDH was decreased relatively. Considering the phosphate removal performance and meeting the first-level discharge standard ($\leq$0.5 $mg \cdot L^{-1}$) in the comprehensive sewage discharge standard of China (GB8978-1996), the optimal dosage of 5 $g \cdot L^{-1}$ was selected in the following study when the phosphate concentration was 30 $mg \cdot L^{-1}$. Under this condition, the phosphate removal rate was 98.6% and the phosphate concentration in the effluent was 0.42

230 mg·L^{-1}.

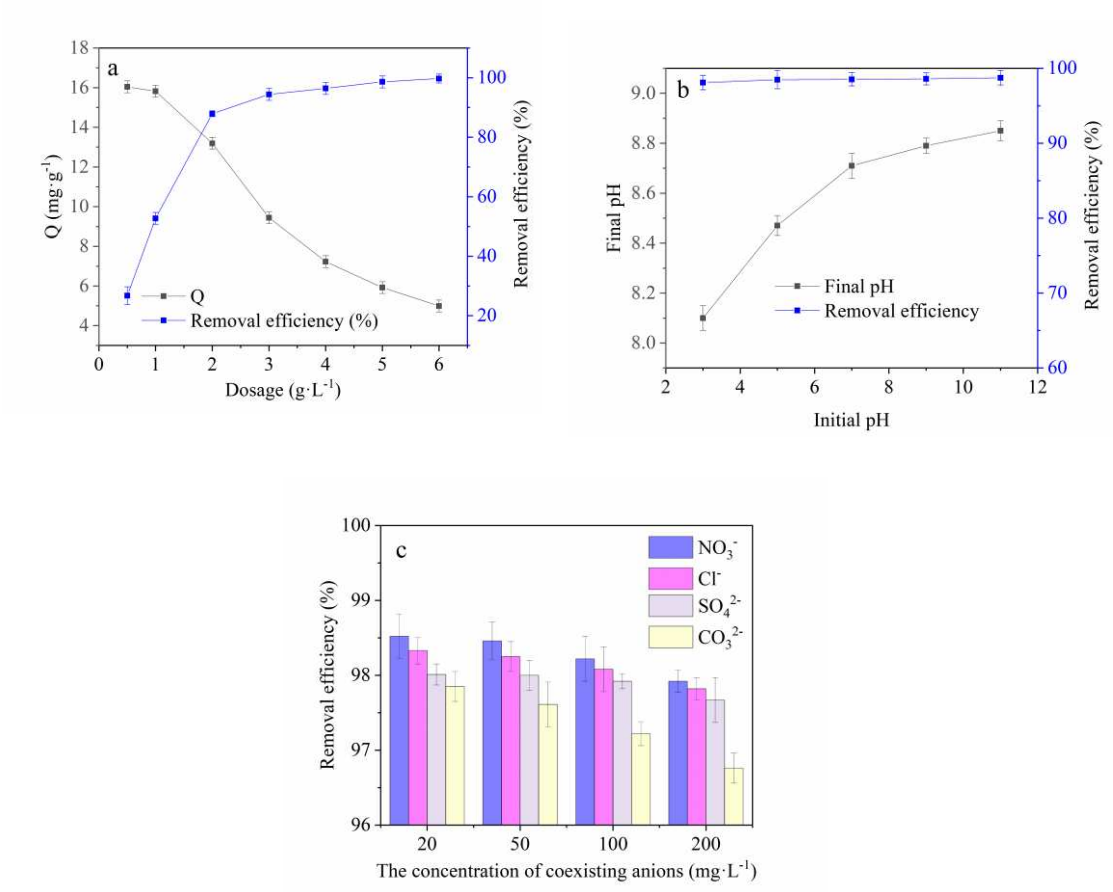

231 Fig. 3 Adsorption performance of CR-LDH towards phosphate as a function of
232 CR-LDH dosage (a), initial pH (b) and of coexisting anions (c).

233 **3.2.2. Effect of initial pH values on phosphate adsorption**

234 pH is deemed as an important factor influencing the physico-chemical adsorption
235 reaction process of adsorbent towards adsorbate because pH will influence the
236 phosphate dissociation equilibria in aqueous solutions (Cheng et al., 2009; Kong et al.,
237 2020; Zhang et al., 2019):

238 $$H_3PO_4 \xleftrightarrow{K_1} H_2PO_4^- + H^+ \xleftrightarrow{K_2} HPO_4^{2-} + 2H^+ \xleftrightarrow{K_3} PO_4^{3-} + 3H^+$$

239 where pK_1=2.15, pK_2=7.20 and pK_3=12.33, respectively. In this study, the effect
240 of initial pH values on phosphate adsorption by CR-LDH were investigated at pH

ranging from 3.0 to 11.0 and the results were shown in Fig. 3b. As shown in Fig. 3b, with the increase of initial pH, the phosphate removal rate increased gradually, but the change range was relatively small. When the pH was in the range of 3.0-11.0 (the main species of phosphate was $H_2PO_4^-$ and HPO_4^{2-}), CR-LDH maintained a high phosphate removal rate. Due to the adsorption free energy of $H_2PO_4^-$ was lower than that of HPO_4^{2-} (Yang et al., 2014), so CR-LDH was more likely to adsorb $H_2PO_4^-$. At pH 3.0 and 11.0, the phosphate removal rate were 98.1% and 98.7%, respectively. This phenomenon is mainly due to that CR-LDH have a certain regulating effect on the pH of the solution. The final pH values were gradually increased after reaction equilibrium and remained ranging from 8.1 to 8.9, indicating that OH^- were released by CR-LDH in the adsorption process under lower pH. While at higher pH values, OH^- was consumed in the transformation process of calcium phosphate precipitation into hydroxyapatite. Considering that the actual water samples are mostly in the neutral range, pH of 7.0 was selected in the follow-up experiments.

3.2.3. Effect of co-existing inorganic anions on phosphate adsorption

Phosphate is not existed alone in wastewater, but may be coexisted with CO_3^{2-}, SO_4^{2-}, NO_3^-, Cl^- and other inorganic anions. In this study, the effect of CO_3^{2-}, SO_4^{2-}, NO_3^-, Cl^- on the adsorption performance of CR-LDH towards phosphate were investigated within co-existing inorganic anions concentration of 20, 50, 100 and 200 $mg \cdot L^{-1}$, respectively. As shown in Fig. 3c, when CO_3^{2-}, SO_4^{2-}, NO_3^-, Cl^- were con-existed in solution, the removal rate of phosphate was deceased in varying degrees. The inhibition effect of co-existing inorganic anions was increased with the

increase of its concentration. Under the same initial concentration of CO_3^{2-}, SO_4^{2-}, NO_3^-, Cl^-, the inhibition order of the above four co-existing ions was as follows: $CO_3^{2-}>SO_4^{2-}>Cl^->NO_3^-$. When the concentration of CO_3^{2-} was 200 $mg\cdot L^{-1}$, the removal rate of CR-LDH towards phosphate was reduced to 96.77% and the effluent phosphate concentration was 0.97 $mg\cdot L^{-1}$. The inhibition effect of co-existing inorganic anions was mainly due to the fact that these anions would compete with phosphate to enter the interlayer structure of CR-LDH in adsorption process, resulting in decrease adsorption sites of the interlayer. The interaction between the inorganic anions with higher valence and the positively charged laminates was stronger, which made it easier to enter the interlayer channels of CR-LDH. As a result, the inhibitory effect of bivalent anion (CO_3^{2-} and SO_4^{2-}) were stronger than that of monovalent anion (NO_3^- and Cl^-), which was consistent with the research results reported in previous publications (Seftel et al., 2018).

3.2.4. Adsorption kinetics

The process of phosphate adsorbed by CR-LDH is a time-dependent reaction. The adsorption behavior of CR-LDH with respect to phosphate as a function of time was studied and the results were shown in Fig. 4. It can be seen that the adsorption of phosphate by CR LDHs can be roughly divided into three stages, namely, the rapid adsorption reaction stage of 0-60 min, the slow adsorption reaction stage of 60-480 min, and the adsorption equilibrium stage after 480 min. At the initial stage of adsorption, the surface of CR-LDH possessed abundant adsorption sites and a large number of phosphate were existed in the solution, leading to the faster adsorption rate

of phosphate by CR-LDH. With the progress of the reaction, the concentration of phosphate was decreased in the solution and numerous adsorption site on the surface of CR-LDH were occupied by phosphate. As a result, the available adsorption sites of CR-LDH were less and the adsorption rate of phosphate was decreased accordingly.

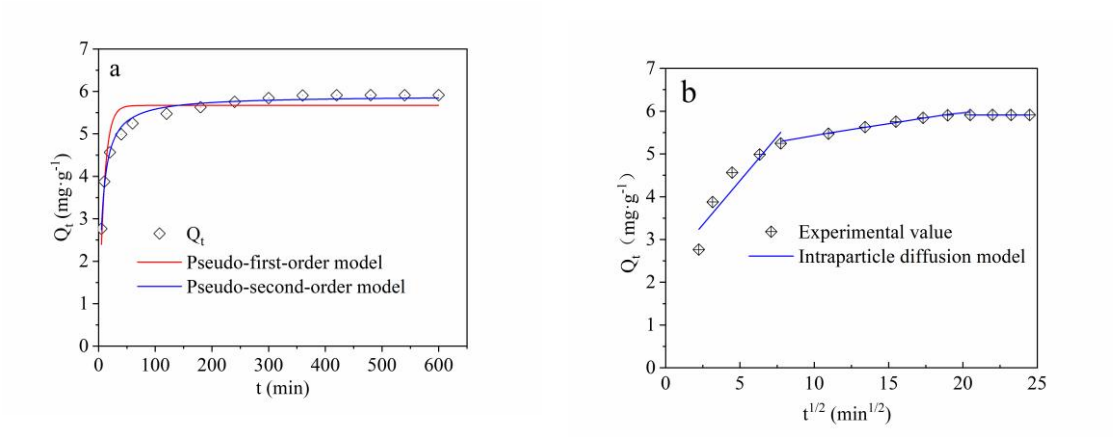

Fig. 4 Fitting results of pseudo-first-order, pseudo-second-order kinetic model (a) and intra-particle diffusion model (b).

To better describe the adsorption process of CR-LDH towards phosphate, pseudo-first-order, pseudo-second-order and intra-particle diffusion kinetic models were adopted in this study. The pseudo-first-order and pseudo-second-order equations are expressed as Eq. (3) and Eq. (4), respectively.

$$Q_t = Q_e(1-e^{-k_1 t}) \quad (3)$$

$$Q_t = \frac{Q_e^{\,2} k_2 t}{1+Q_e k_2 t} \quad (4)$$

where t (min) represents the adsorption time; Q_t is the adsorption amount of phosphate adsorbed by CR-LDH at time t, mg·g^{-1}; Q_e represents the equilibrium adsorption capacity, mg·g^{-1}; k_1 (min^{-1}) and k_2 (g·mg^{-1}·min^{-1}) donate the pseudo-first-order and pseudo-second-order rate constants, respectively. As illustrated

299 in Fig. 4a and Table 2, the pseudo-second-order kinetic model (R^2=0.989) better fitted
300 than the pseudo-second-order kinetic model (R^2=0.896) for phosphate adsorption on
301 CR-LDH, suggesting that the adsorption of phosphate onto CR-LDH was mainly
302 controlled by chemical adsorption through sharing or exchanging electrons, thus
303 forming valence force for adsorption (Cao et al., 2020).

304 To determine the adsorption rate limiting step, intra-particle diffusion model was
305 used to fitting the adsorption experimental results. The intra-particle diffusion model
306 can be expressed as follows:

$$Q_t = k_3 t^{1/2} + C \quad (5)$$

307 where k_3 represents the intra-particle diffusion rate constant ($mg\cdot(g\ min^{1/2})^{-1}$) and C is
308 the constant related to the thickness of the boundary layer ($mg\cdot g^{-1}$).

309 Table 2 Fitting results of kinetic model.

Kinetic model	Parameter	Value
Pseudo-first-order kinetic model	Q_e	5.67
	k_1	0.10967
	R^2	0.896
Pseudo-second-order kinetic model	Q_e	5.90
	K_2	0.0293
	R^2	0.989
Intra-particle diffusion	C1	2.3151
	R_1^2	0.8689
	k_{31}	0.4119

C2	4.8779
k_{32}	0.0538
R_2^2	0.970
C3	5.9009
k_{33}	0.0005
R_3^2	0.6439

According to intra-particle diffusion kinetic model, if the adsorption rate is only determined by the intra-particle diffusion, the Q_t-$t^{1/2}$ curve will be a straight line with C value of zero. As shown in Fig. 4b and Table 2, the adsorption experimental results of CR-LDH towards phosphate presented a linear relationship in three stages and value of C was not zero, suggesting that intra-particle diffusion was not the solely speed limiting step. The adsorption process of CR-LDH with respect to phosphate could be divided into three stages: film diffusion stage, intra-particle diffusion stage and adsorption equilibrium stage. The film diffusion stage which occurred on the initial of the reaction of 0-60 min was a rapid adsorption stage. Phosphate could transfer to the abundant adsorption sites on the surface of CR-LDH through film diffusion to achieve rapid adsorption. The intra-particle diffusion stage happened on 60-480 min was a gradual adsorption stage. In this stage, phosphate reached the adsorption sites inside the pores of the CR-LDH with the happening of intra-particle diffusion. The third stage was adsorption equilibrium stage (>480 min) and the adsorption driving force was relatively weak due to the fact that there were fewer adsorption sites in the solution and the number of free phosphate radicals was very

limited. The obtained C value followed the sequence of $C_1<C_2<C_3$, indicating that the boundary layer thickness of CR-LDH was increased with the proceed of adsorption reaction of CR-LDH towards phosphate.

3.2.5. Adsorption isotherms

Adsorption isotherms of phosphate removed by CR-LDH were investigated within different concentration of phosphate ranging from 0 to 150 $mg \cdot L^{-1}$ at three different temperatures (15, 25 and 35 ^oC) and the results were shown in Fig. 5. As exhibited in Fig. 5, with the increasing of phosphate's initial concentration, the adsorption capacity of CR-LDH towards phosphate was increased. When the initial concentration of phosphate was at a relatively low level, the adsorption sites on CR-LDH could ensure that most of the phosphate in the solution was removed, and the corresponding phosphate adsorption capacity of CR-LDH showed a linear upward trend. With the further increase of the initial phosphate concentration, more and more adsorption sites were occupied by phosphate radicals, and the number of free adsorption sites was decreased, leading to the decrease in the tangent slope of the phosphate adsorption curve.

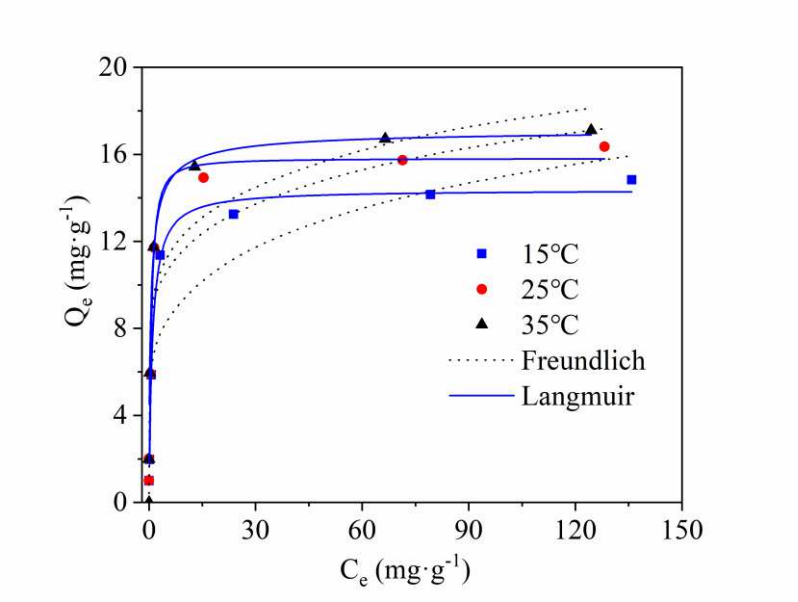

Fig. 5 Isotherms of phosphate adsorption on CR-LDH.

Langmuir and Freundlich isotherm models were conducted to simulate the adsorption experimental data of phosphate adsorbed by CR-LDH. The equation of Langmuir (chemical adsorption model of single molecular layer) and Freundlich (empirical model) isotherm models can be expressed as (Kong et al., 2019):

$$Q_e = \frac{Q_{max} b C_e}{1 + b C_e} \quad (8)$$

$$Q_e = K_F C_e^{1/n} \quad (9)$$

where C_e represents equilibrium concentration of phosphate, mg·L^{-1}; Q_{max} is the maximum adsorption capacity, mg·g^{-1}; b is the affinity coefficient, L·mg^{-1}; K_F and n represent the constants of Freundlich isotherm model.

The fitting results of experimental data of Langmuir and Freundlich isotherm models are exhibited in Fig. 5 and Table 3. Compared to Freundlich isotherm model, Langmuir isotherm model (R^2>0.98) was more suitable to fit the adsorption process of phosphate adsorbed onto CR-LDH which indicated that the adsorbed phosphate had

no interaction with each other and were distributed on the surface of CR-LDH as a molecular layer. The maximum adsorption capacity values calculated by Langmuir isotherm were close to the experimental data. When the temperature increased from 15 to 35 ºC, the maximum adsorption capacity of CR-LDH towards phosphate were enhanced from 14.41 to 16.59 $mg \cdot g^{-1}$, indicating that high temperature had a beneficial effect on adsorption of phosphate. Comparison of the adsorption ability of different adsorbents towards phosphate is provided in Table 4. It can be seen that the maximum adsorption capacity of CR-LDH was in the middle level. In light of the cost of the adsorbent and the reuse of industrial waste-carbide slag, CR-LDH is still considered as a potential environmental friendly adsorbent. The n values of Freundlich isotherm model were all higher than 1, suggesting that the adsorption process of CR-LDH with respect to phosphate was easily implemented.

Table 3 Isotherm fitting results of phosphorus removal by CR-LDH.

Temperature	Q_{max}	Langmuir			Freundlich	
			R^2	K_F		R^2
（ºC）	$(mg \cdot g^{-1})$	b			n	
15	14.41	1.06	0.994	6.87	5.83	0.889
25	16.06	1.53	0.989	9.45	8.12	0.941
35	16.59	2.19	0.993	9.97	8.07	0.955

Table 4 Comparison of the adsorption ability of different LDHs towards phosphate.

Adsorbents	Maximum adsorption amount $(mg \cdot g^{-1})$	References
Zn-Al LDH	41.26	(Cheng et al., 2010)

Mg-Al LDH	31.30	(Yang et al., 2014)
Zn-Al LDH	68.40	(Yang et al., 2014)
Calcined MgMn-LDHs	7.30	(Chitrakar et al., 2005)
Mg-Al LDH (granular)	47.30	(Kuzawa et al., 2006)
CR-LDH	16.06	This study

3.2.6. Adsorption thermodynamics

Adsorption thermodynamics analysis were also carried out to describe the adsorption process of phosphate adsorbed by CR-LDH. The adsorption thermodynamics formula can be expressed as follows:

$$\Delta G^0 = -RT\ln K^0 \quad (10)$$

$$\ln K^0 = \frac{\Delta S^0}{R} - \frac{\Delta H^0}{RT} \quad (11)$$

where ΔG^0 is the Gibbs free energy, $KJ\cdot mol^{-1}$; R represents the is the constant of perfect gas and R=8.314 $J\cdot mol^{-1}\cdot K^{-1}$; T is the absolute temperature of solution, K; ΔS^0 represents the entropy change, $J\cdot mol^{-1}\cdot K^{-1}$; ΔH^0 is the enthalpy change, $KJ\cdot mol^{-1}$ and K^0 is the standard equilibrium constant. Because the adsorption process of CR-LDH with respect to phosphate fitted Langmuir isotherm model well with $R^2>0.98$, so the Langmuir constant of b could be calculated as K^0.

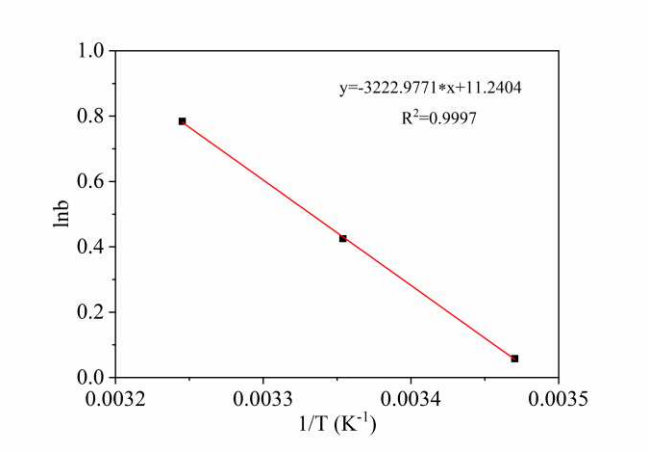

379

380 Fig. 6 lnb and 1/T relationship curve of CR-LDH adsorption phosphorus.

381 As shown in Fig. 6 and Table 5, the values of ΔG^0 were all less than zero which
382 suggested the adsorption process of phosphate by CR-LDH were spontaneous reaction.
383 The absolute values of ΔG^0 became more positive with the increasing of temperature,
384 suggesting that higher temperature was more conductive to the adsorption of
385 CR-LDH towards phosphate. The positive ΔH^0 of 26.21 KJ·mol^{-1} implied that the
386 adsorption of phosphate by CR-LDH were endothermic and this finding was in
387 agreement with the results that the adsorption capacities of CR-LDH were enhanced
388 with the increasing of temperature. The positive ΔS^0 of 91.45 J·mol^{-1}·K^{-1} indicated
389 that the randomness at the solid-solution interface was increased which was due to the
390 adsorption reaction of phosphate adsorbed by CR-LDH.

391 Table 5 Thermodynamic results of phosphorus adsorbed by CR-LDH.

Temperature（K）	△G（KJ·mol^{-1}）	△H（KJ·mol^{-1}）	△S（J·mol^{-1}·K^{-1}）
288.15	-0.140		
298.15	-1.054	26.21	91.45
308.15	-2.008		

3.2.7. Application of CR-LDH to practical phosphate-containing wastewater

To investigate the applicability of CR-LDH for the removal of phosphate in practical phosphate-containing wastewater, the untreated wastewater in the sewage well of a machinery factory in Shenyang is selected and analyzed. Phosphating is an important process in the pretreatment process of coating surface in mechanical processing plants. A large number of phosphorus-containing agents are needed in the phosphating process, and the phosphate content of phosphating wastewater often exceeds the standard. The soluble orthophosphate forms in phosphating wastewater account for about 87.8% of total soluble phosphorus, which is comparable with the use of simulated phosphorus containing wastewater as experimental water. The photos and water quality parameters of practical phosphate-containing wastewater before CR-LDH adsorption and after CR-LDH adsorption were given in Fig. S3 and Table 6, respectively.

Table 6 Water quality parameters of practical phosphate-containing wastewater before and after CR-LDH adsorption ($mg \cdot L^{-1}$, except for pH).

Process	pH	COD_{cr}	Turbidity (NTU)	NH_4^+-N	PO_4^{3-}-P
Before CR-LDH adsorption	7.32	92.0	30.7	62	9.8
After CR-LDH adsorption	7.89	53	7	49.16	0.48

First-class standard of national discharge standards	6-9	60	1	5	0.5

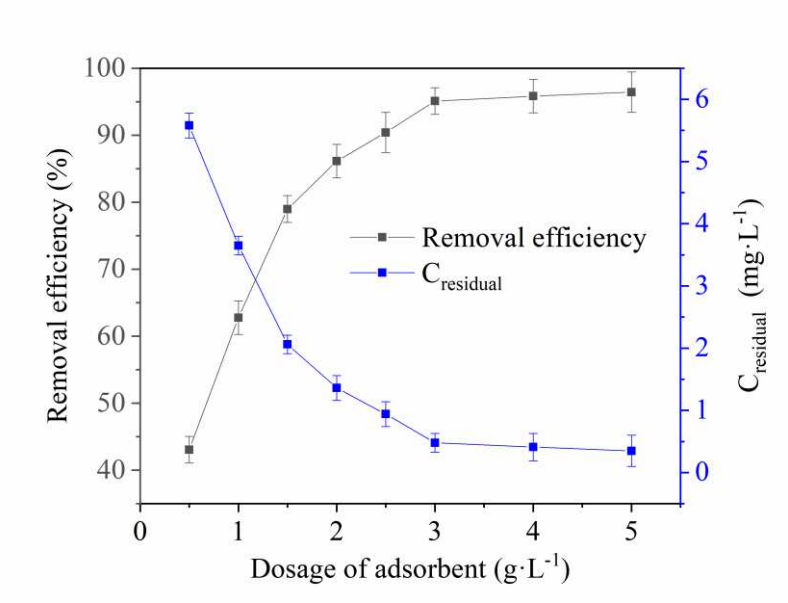

Fig. 7 Effect of dosages on the removal of phosphate from practical phosphate-containing wastewater.

In the applicability of CR-LDH test, 0.5, 1, 1.5, 2, 3, 4 and 5 g/L of CR-LDH were added into the 100 mL practical phosphate-containing wastewater for the adsorption experiments, respectively. After adsorption for 8 h at 25 ºC, the samples were filtered through 0.45 μm cellulose filtered membrane and then diluted for further phosphate analysis. As exhibited in Fig. 7 and Table 5, the residual phosphate of practical wastewater was decreased gradually as the increase of CR-LDH dosage, while the phosphate removal rate was increased first and then stabilized. When the dosage of CR-LDH was 3 g/L, the residual phosphate concentration was 0.48 mg·L^{-1} and the corresponding removal rate was 95.1%, which met the first class discharge

standard (≤0.5 $mg \cdot L^{-1}$) in the integrated wastewater discharge standard (GB8978-1996). The effluent pH met the discharge standard and the COD, turbidity and NH_4^+-N were reduced by 42.39%, 77.20% and 20.71%, respectively. The above results indicated that CR-LDH had great potential for adsorbing phosphate from practical phosphate-containing wastewater.

3.3. Adsorption mechanism

In order to clarify the adsorption mechanism, FT-IR was used to find out the functional groups' changes of CR-LDH before and after adsorption of phosphate. As shown in Fig. S4, the peak at 3415.75 cm^{-1} and 1637.79 cm^{-1} were assigned to the stretching and bending vibration of the -OH in the CR-LDH and interstitial water molecules, respectively. After adsorbed phosphate, the peaks at 1003.28 cm^{-1} and 548 cm^{-1} appeared which were attributed to the stretching and bending vibration of phosphate. The band at 874 cm^{-1} belonged to the vibration of P-O in HPO_4^{2-}, indicating that effective adsorption of phosphate by CR-LDH was existed.

The XRD spectra of CR-LDH after adsorption of phosphate is shown in Fig. 8. Compared to XRD pattern of CR-LDH before adsorption of phosphate, the diffraction peak intensity of boehmite was decreased and the characteristic diffraction peak of brucite was disappeared. New diffraction peaks of $Ca_2P_2O_7$, Ca_2P_2, $Mg_3(PO_4)_2$ were appeared which might be due to that phosphate entered into the layered structure of CR-LDH after the adsorption process and Ca^{2+} dissolved on the surface combined with HPO_4^{2-} hydrolyzed to form $CaHPO_4$. After that, $CaHPO_4$ was polymerized and dehydrated to form $Ca_2P_2O_7$ precipitation. The peaks at 2θ of 26.47^0 and 39.49^0 were

attributed to CaO. The adsorption peak of $CaCO_3$ was appeared at 2θ of 43.14^0. The appearance of peaks at 2θ of 33.24^0, 35.73^0 and 54.21^0 identified the existence of Fe_2O_3. The reason for the existence of the above metal oxides in the XRD pattern of CR-LDH after adsorption of phosphate was due to that the raw material of carbide slag was industrial waste and the metal oxide didn't fully react during the preparation process of CR-LDH.

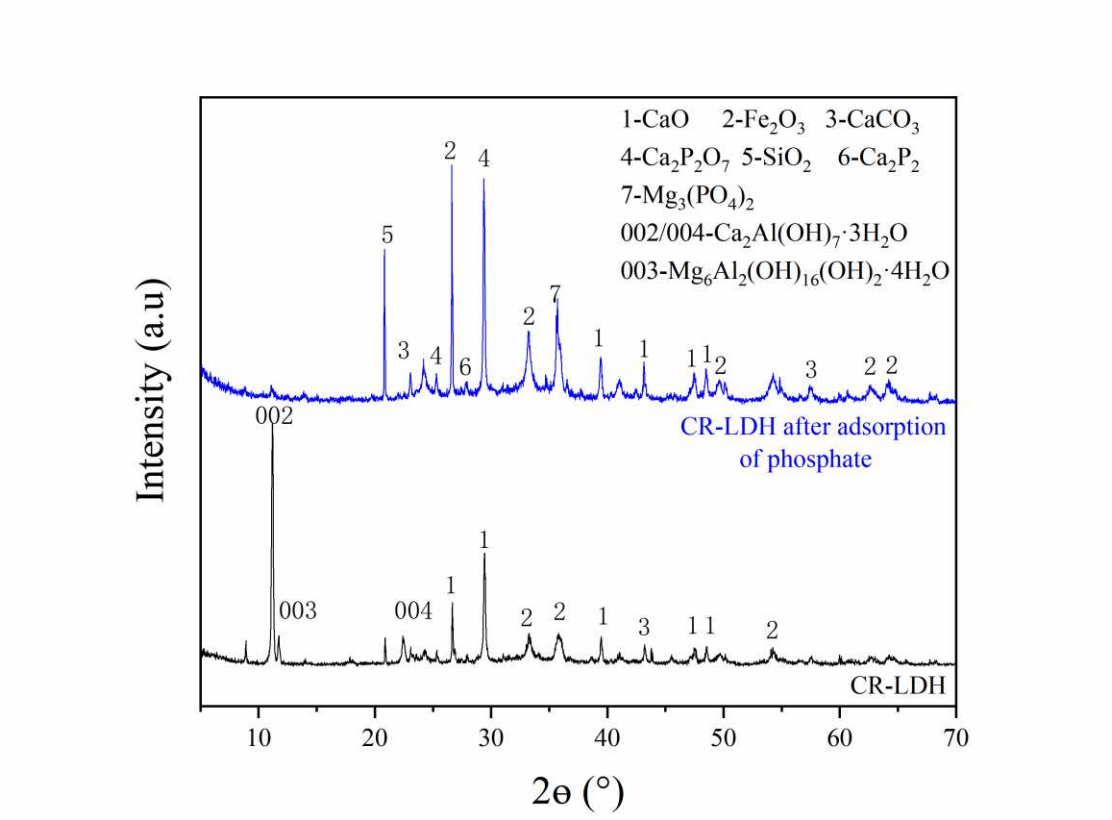

Fig. 8 XRD pattern of CR-LDH and after adsorption of phosphate.

According to the EDS results (Fig. 9a and Table 1), non-metallic P element was appeared in CR-LDH after adsorption of phosphate, indicating that the surface of the CR-LDH composite could adsorb phosphate by surface adsorption, surface complexation, electrostatic attraction and chemical precipitation. The SEM images of CR-LDH after adsorption of phosphate (Fig. 9b and Fig. 9c) exhibited a relatively flat,

irregular block morphology and the surface gap of CR-LDH was filled, leading to the increase in the specific surface area which was conductive for the adsorption process. During the adsorption process, the free metal cations might be combined with PO_4^{3-} and hydroxyl groups to form phosphate or other metal oxides and then deposited on the surface of the adsorbent. ɵ

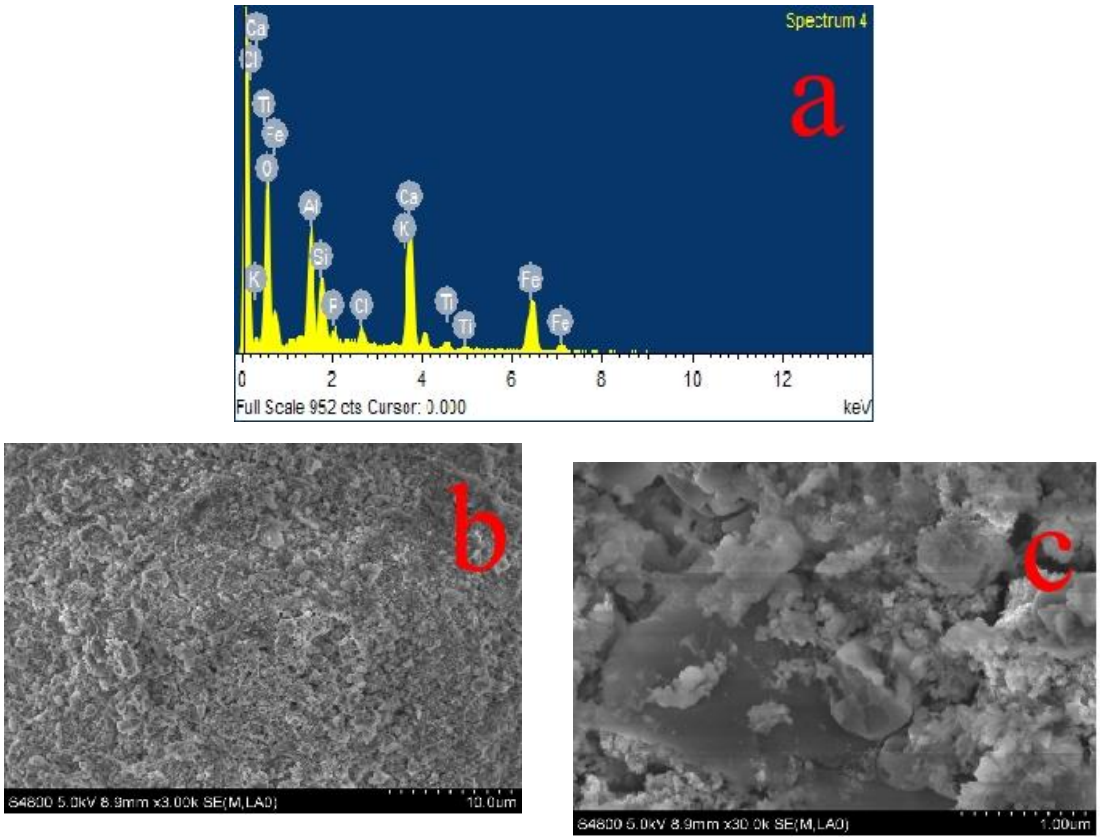

Fig. 9 EDS of CR-LDH after adsorption of phosphate (a) and SEM of CR-LDH after adsorption of phosphate (b and c).

Based on the adsorption experimental results and characterization analysis, we could infer that the adsorption of phosphate by CR-LDH might be through the following four interactions: (1) physical adsorption; The strength of physical adsorption mainly depends on the specific surface area and pore size distribution of adsorbent. Generally, the larger the specific surface area of adsorbent, the higher the

adsorption capacity of physical adsorption. CR-LDH with surface area of 42.46 $m^2 \cdot g^{-1}$ had a lamellar structure due to the large number of gaps on the surface and the relatively rough surface (Fig. 2), providing a great quantity of active adsorption sites for the adsorption of phosphate. Thus, part of phosphate could be adsorbed on the surface of CR-LDH by van der Waals force of physical adsorption. (2) ion exchange; The exchangeability of interlayer anions is one of the important properties of LDHs. Some anions in the aqueous solution will enter the material ion layer, while the anions originally in the ion layer will transfer to the aqueous solution. The interlayer anions in the layered structure of CR-LDH in solution might be replaced by anions with stronger exchange performance to achieve partial adsorption of phosphate. (3) anion intercalation; Since CR-LDH laminates are positively charged, the anions in the solution will enter the layers of CR-LDH to balance the structure and electrical properties of the laminates, so anion intercalation plays an important role in the process of phosphate removed by CR-LDH. This inference was consistent with XRD results that the intensity of the hydrocalumite diffraction peak was decreased after the adsorption of phosphate, the characteristic diffraction peak of magnesia was disappeared, and the diffraction peak of $Ca_2P_2O_7$ was appears, indicating that part of phosphate entered into the interlayer structure of CR-LDH. The phosphate on the surface of CR-LDH would form phosphorus-containing precipitate with dissolved Mg^{2+} and Ca^{2+}. (4) chemical precipitation. The free metal cations (Ca^{2+}, Al^{3+}, Fe^{3+}, etc) produced by CR-LDH would be combined with phosphate to form various precipitates and then deposited on the surface of adsorbent, leading to the flat surface

of CR-LDH after adsorption of phosphate (Fig. 9b). The appearance of $Ca_2P_2O_7$ in the XRD pattern of CR-LDH after adsorption of phosphate suggested that Ca^{2+}dissolved from CR-LDH was combined with HPO_4^{2-} to form $CaHPO_4$ and then polymerize, dehydrated to obtain $Ca_2P_2O_7$ precipitate (Fig. 8). The detection of P element in the EDS of CR-LDH after adsorption of phosphate also indicated that chemical prchemical precipitation was occurred in the process of phosphate adsorbed by CR-LDH (Fig. 9a).

4. Conclusion

In this study, adsorbent of CR-LDH were successfully designed via a simple method by using calcium carbide slag and red mud as raw materials. Characterization results showed that the synthesized CR-LDH had typical properties of LDH. The experimental data of phosphate adsorbed by CR-LDH could be well fitted by pseudosecond-order model and Langmuir isotherm model with theoretical maximum adsorption capacity of 16.06 $mg \cdot g^{-1}$ at 25 ^oC, suggesting that it's a chemical and monolayer adsorption process. Based on the adsorption experimental results and characterization analysis, the adsorption of phosphate by CR-LDH was assumed to be through physical adsorption, ion exchange, anion intercalation and chemical precipitation. In brief, the CR-LDH prepared from calcium carbide slag and red mud was a effective adsorbent for treating practical phosphate-containing wastewater, which is helpful for the reuse of industrial waste resources, the reduction of environmental pollutants of phosphate and the protection of the environment.

Ethics approval and consent to participate

Not applicable.

Consent for publication

Not applicable.

Authors Contributions

Liping Xiao: Resources, Methodology, Investigation, Supervision, Conceptualization, Project administration, Writing - review & editing. Yan Li: Methodology, Investigation, Resources, Writing - review & editing. Qiaoping Kong: Writing - original draft, Writing - review & editing, Methodology, Investigation, Resources. Yunlong Lan: review & editing.

Availability of data and materials

Not applicable.

Competing Interest

The authors declare that they have no known competing financial interests or personal relationships that could have appeared to influence the work reported in this paper.

Acknowledgments

This work was supported by the National Natural Science Foundation of China (NO. 51474122 and NO. 51174267) and the Key projects of scientific research fund of Liaoning Provincial Department of Education (NO. ZL002)

References:

Bacelo, H., Pintor, A.M.A., Santos, S.C.R., Boaventura, R.A.R., Botelho, C.M.S., 2020. Performance and prospects of different adsorbents for phosphorus uptake and recovery

533 from water. *CHEMICAL ENGINEERING JOURNAL*, 381, 122566.
534 Cao, H., Wu, X., Syed-Hassan, S.S.A., Zhang, S., Mood, S.H., Milan, Y.J.,
535 Garcia-Perez, M., 2020. Characteristics and mechanisms of phosphorous adsorption by
536 rape straw-derived biochar functionalized with calcium from eggshell.
537 *BIORESOURCE TECHNOLOGY*, 318.
538 Cheng, S., Shao, L., Ma, J., Xia, X., Liu, Y., Yang, Z., Yang, C., Li, S., 2019.
539 Simultaneous removal of phosphates and dyes by Al-doped iron oxide decorated MgAl
540 layered double hydroxide nanoflakes. *ENVIRONMENTAL SCIENCE. NANO*, 6,
541 2615-2625.
542 Cheng, X., Huang, X., Wang, X., Sun, D., 2010. Influence of calcination on the
543 adsorptive removal of phosphate by Zn-Al layered double hydroxides from excess
544 sludge liquor. *JOURNAL OF HAZARDOUS MATERIALS*, 177, 516-523.
545 Cheng, X., Huang, X., Wang, X., Zhao, B., Chen, A., Sun, D., 2009. Phosphate
546 adsorption from sewage sludge filtrate using zinc-aluminum layered double hydroxides.
547 *JOURNAL OF HAZARDOUS MATERIALS*, 169, 958-964.
548 Chitrakar, R., Tezuka, S., Sonoda, A., Sakane, K., Ooi, K., Hirotsu, T., 2005.
549 Adsorption of phosphate from seawater on calcined MgMn-layered double hydroxides.
550 *JOURNAL OF COLLOID AND INTERFACE SCIENCE*, 290, 45-51.
551 Dox, K., Pareijn, R., Everaert, M., Smolders, E., 2019. Phosphorus recycling from
552 urine using layered double hydroxides: A kinetic study. *APPLIED CLAY SCIENCE*,
553 182, 105255.
554 Guo, Z., Li, J., Guo, Z., Guo, Q., Zhu, B., 2017. Phosphorus removal from aqueous

555 solution in parent and aluminum-modified eggshells: thermodynamics and kinetics,
556 adsorption mechanism, and diffusion process. *ENVIRONMENTAL SCIENCE AND*
557 *POLLUTION RESEARCH*, 24, 14525-14536.
558 Hu, P., Zhang, Y., Lv, F., Tong, W., Xin, H., Meng, Z., Wang, X., Chu, P.K., 2017.
559 Preparation of layered double hydroxides using boron mud and red mud industrial
560 wastes and adsorption mechanism to phosphate. *WATER AND ENVIRONMENT*
561 *JOURNAL : WEJ*, 31, 145-157.
562 Jia, Z., Hao, S., Lu, X., 2018. Exfoliated Mg-Al-Fe layered double
563 hydroxides/polyether sulfone mixed matrix membranes for adsorption of phosphate
564 and fluoride from aqueous solutions. *JOURNAL OF ENVIRONMENTAL SCIENCES*,
565 70, 63-73.
566 Jiang, Y., Chen, Y., Du, Q., Shi, J., 2019. Adsorption of different forms of phosphorus
567 on modified corn bracts. *WATER ENVIRONMENT RESEARCH*, 91, 748-755.
568 Jiang, Y., Li, A., Deng, H., Ye, C., Li, Y., 2019. Phosphate adsorption from wastewater
569 using ZnAl-LDO-loaded modified banana straw biochar. *ENVIRONMENTAL*
570 *SCIENCE AND POLLUTION RESEARCH*, 26, 18343-18353.
571 Kong, Q., Preis, S., Li, L., Luo, P., Hu, Y., Wei, C., 2020. Graphene oxide-terminated
572 hyperbranched amino polymer-carboxymethyl cellulose ternary nanocomposite for
573 efficient removal of heavy metals from aqueous solutions. *INTERNATIONAL*
574 *JOURNAL OF BIOLOGICAL MACROMOLECULES*, 149, 581-592.
575 Kong, Q., Shi, X., Ma, W., Zhang, F., Yu, T., Zhao, F., Zhao, D., Wei, C., 2021.
576 Strategies to improve the adsorption properties of graphene-based adsorbent towards

heavy metal ions and their compound pollutants: A review. *JOURNAL OF HAZARDOUS MATERIALS*, 415, 125690-125690.

Kong, Q., Wei, J., Hu, Y., Wei, C., 2019. Fabrication of terminal amino hyperbranched polymer modified graphene oxide and its prominent adsorption performance towards Cr(VI). *JOURNAL OF HAZARDOUS MATERIALS*, 363, 161-169.

Kuzawa, K., Jung, Y., Kiso, Y., Yamada, T., Nagai, M., Lee, T., 2006. Phosphate removal and recovery with a synthetic hydrotalcite as an adsorbent. *CHEMOSPHERE*, 62, 45-52.

Li, X., Xie, Q., Kuang, Y., Wu, D., 2021. Coupled influence of pH and dissolved organic carbon on the immobilization of phosphorus by lanthanum-modified zeolite. *CHEMOSPHERE*, 274.

Liu, C., Zhang, M., Pan, G., Lundehoj, L., Nielsen, U.G., Shi, Y., Hansen, H.C.B., 2019. Phosphate capture by ultrathin MgAl layered double hydroxide nanoparticles. *APPLIED CLAY SCIENCE*, 177, 82-90.

Razmi, B., Ghasemi-Fasaei, R., 2018. Investigation of Taguchi optimization, equilibrium isotherms, and kinetic modeling for phosphorus adsorption onto natural zeolite of clinoptilolite type. *ADSORPTION SCIENCE & TECHNOLOGY*, 36, 1470-1483.

Samaraweera, H., Sharp, A., Edwards, J., Jr. Pittman, C.U., Zhang, X., Hassan, E.B., Thirumalai, R.V.K.G., Warren, S., Reid, C., Mlsna, T., 2021. Lignite, thermally-modified and Ca/Mg-modified lignite for phosphate remediation. *SCIENCE OF THE TOTAL ENVIRONMENT*, 773.

599 Seftel, E.M., Ciocarlan, R.G., Michielsen, B., Meynen, V., Mullens, S., Cool, P., 2018.
600 Insights into phosphate adsorption behavior on structurally modified ZnAl layered
601 double hydroxides. *APPLIED CLAY SCIENCE*, 165, 234-246.
602 Tie, J., Chen, D., Wan, Y., Yan, C., Zhang, X., 2013. Adsorption removal of phosphorus
603 from aqueous solution by heat-activated alum sludge. *ASIAN JOURNAL OF*
604 *CHEMISTRY*, 25, 9129-9134.
605 Wang, Z., Miao, R., Ning, P., He, L., Guan, Q., 2021. From wastes to functions: A paper
606 mill sludge-based calcium-containing porous biochar adsorbent for phosphorus
607 removal. *JOURNAL OF COLLOID AND INTERFACE SCIENCE*, 593, 434-446.
608 Yang, F., Zhang, S., Sun, Y., Tsang, D.C.W., Cheng, K., Ok, Y.S., 2019. Assembling
609 biochar with various layered double hydroxides for enhancement of phosphorus
610 recovery. *JOURNAL OF HAZARDOUS MATERIALS*, 365, 665-673.
611 Yang, K., Yan, L., Yang, Y., Yu, S., Shan, R., Yu, H., Zhu, B., Du, B., 2014. Adsorptive
612 removal of phosphate by Mg-Al and Zn-Al layered double hydroxides: Kinetics,
613 isotherms and mechanisms. *SEPARATION AND PURIFICATION TECHNOLOGY*, 124,
614 36-42.
615 Zhang, J., Xia, Q., Hong, X., Chen, J., Liu, D., 2021. Synthesis of layered double
616 hydroxides with nitrate and its adsorption properties of phosphate. *WATER SCIENCE*
617 *AND TECHNOLOGY*, 83, 100-110.
618 Zhang, Z., Yan, L., Yu, H., Yan, T., Li, X., 2019. Adsorption of phosphate from aqueous
619 solution by vegetable biochar/layered double oxides: Fast removal and mechanistic
620 studies. *BIORESOURCE TECHNOLOGY*, 284, 65-71.

621 Zhu, D., Yang, H., Chen, X., Chen, W., Cai, N., Chen, Y., Zhang, S., Chen, H., 2021.
622 Temperature-dependent magnesium citrate modified formation of MgO nanoparticles
623 biochar composites with efficient phosphate removal. *CHEMOSPHERE*, 274.
624

Supplementary Files

This is a list of supplementary files associated with this preprint. Click to download.

- SupplementaryMaterial.docx